A Distributed Control Architecture for Global System Economic Operation in Autonomous Hybrid AC/DC Microgrids

Pengfeng Lin, *Student Member, IEEE*, Chi Jin, Jianfang Xiao, *Member, IEEE*, Xiaoqiang Li, *Member, IEEE*, Donghan Shi, *Student Member, IEEE*, Yi Tang, *Member, IEEE*, and Peng Wang, *Fellow, IEEE*

***Abstract*—It is renowned that the entire power system operation cost can be minimized when distributed generators (DGs) have the same incremental costs (ICs). This paper proposes a distributed control architecture for a hybrid ac/dc microgrid (MG) to realize global system economic operation. The architecture consists of two levels. In the first level, the ac frequency-IC (f_{ac}-IC) droop and the dc bus voltage-IC (V_{dc}-IC) droop are employed in the ac and dc subgrids, respectively. With the synchronization of f_{ac} and V_{dc}, DG ICs in each subgrid will be equalized. However, the droops will inevitably cause deviations of f_{ac} and V_{dc}. Then a distributed control canonical form (DCCF), which provides a generalized method for f_{ac} and V_{dc} recoveries, is proposed in the second level. The DCCF allows DGs to communicate only with their neighbors, thus alleviating the communication burdens and enhancing the system scalability. Due to the presence of DCCF, f_{ac} and V_{dc} fluctuations, which naturally indicate subgrid loading conditions, are invisible. An original relative loading index (RLI) is proposed to extract the hidden loading condition of each subgrid even though f_{ac} and V_{dc} are clamped as constants. By using RLI, the power reference of the bidirectional interlinking converter can be easily defined. All DG ICs the hybrid MG converge to the same value in the steady state. The feasibility and effectiveness of the proposed control architecture are verified by simulations and RT-LAB hardware in loop tests.**

***Index Terms*—Hybrid ac/dc microgrid, distributed control, global system economic operation, power management.**

I. Introduction

PROGRESSIVE developments in power electronics encourage high penetration of heterogeneous renewable energy sources (RESs) and nonconventional microsources in electrical power systems [1]. These sources can be interconnected together and further form entities which are known as microgrids (MGs). Many academic efforts have been given to alternative current (AC) MGs due to the dominant role of AC power delivery in the traditional generation, transmission, and distribution networks. On the other hand, direct current (DC) MGs become increasingly popular in contemporary applications since many renewable energy sources (RESs), energy storages (ESs), and loads (e.g., motor drives and electrical vehicles chares) are naturally DC [2]. To merge advantages of AC and DC MGs, a favorable choice is to construct a hybrid AC/DC MG wherein AC and DC subgrids are intertied through bidirectional interlinking converters (BICs). By this means, AC and DC subgrids serve as the energy backup for each other, and thus the system reliability and stability can be greatly improved [3].

Normally, different distributed generators (DGs) in a MG have distinctive generation costs. Proper DGs dispatch schemes should be adopted to minimize the entire operation cost. In general, system optimization can be realized in centralized and decentralized ways. For the former, decision making for power allocation among DGs is accomplished in a central controller where time-consuming algorithms, including Lagrangian relaxation, genetic algorithm [4], quadratic programming [5] and robust two-stage coordination [6], are employed. Some other centralized methods taking into account of droop controllers can also be found in [7]–[9]. Although these algorithms are viable and effective, it is worth noting that the plausible performances of the centralized optimization may be compromised by the potential inaccuracy of load forecasting and the improper prediction of RES generations. Moreover, the centralized approaches are also vulnerable to the intensive communication and single point of failures.

To overcome the above difficulties, decentralized economic dispatch mechanisms, which do not rely on communication networks, are widely studied. For instance, in [10], a decentralized self-optimizing control is proposed to regulate the DG powers according to their respective generation costs, but plug-and-play (PnP) properties are not expounded. In [11], the costlier DGs are simply turned off to reduce the operation cost in the case of light load. By extending conventional droop concepts, a cost-based droop scheme is proposed in [19] where the remarkable decrease of total generation cost can be achieved.

Manuscript received September 27, 2017; revised January 4, 2018 and February 2, 2018; accepted February 9, 2018. Date of publication February 13, 2018; date of current version April 19, 2019. This work was supported by the Singapore Economic Development Board through Project Renewable Energy Integration Demonstrator-Singapore under Grant S14-1475-RF-LLF Urban. Paper no. TSG-01399-2017. *(Corresponding author: Chi Jin.)*

P. Lin, C. Jin, J. Xiao, and D. Shi are with ERI@N, Singapore 637141 (e-mail: linp0010@e.ntu.edu.sg; jinchi@ntu.edu.sg; jfxiao@ntu.edu.sg; dhshi@ntu.edu.sg).

X. Li is with the School of Electrical and Power Engineering, China University of Mining and Technology, Xuzhou 221116, China (e-mail: xqlcumt@163.com).

Y. Tang and P. Wang are with the School of Electrical and Electronic Engineering, Nanyang Technological University, Singapore 639798 (e-mail: yitang@ntu.edu.sg; epwang@ntu.edu.sg).

Color versions of one or more of the figures in this paper are available online at http://ieeexplore.ieee.org.

Digital Object Identifier 10.1109/TSG.2018.2805839

However, the scheme fails to obtain the optimal cost saving in all possible operating situations. To address this issue, incremental cost (IC) based droops are illustrated in [14] and [15] to minimize the MG cost in a completely decentralized manner. Nonetheless, the common shortcoming of decentralized methods is that the frequency and voltage deviations cannot be properly eliminated.

In an autonomous hybrid AC/DC MG, floating AC frequency (f_{ac}) and DC bus voltage (V_{dc}) could cause damages to those frequency-/ voltage- sensitive loads, and even result in whole system collapse. Furthermore, when the AC and DC subgrids are integrated to the main grids, synchronization with the mains would also require f_{ac} and V_{dc} to stabilize at their nominal values. For restorations of f_{ac} and V_{dc}, both hierarchical frameworks and distributed control strategies are extensively explored in the literature. The former ones are not recommended for those MGs with high reliability requirements since the implementation of energy management entirely depends on central controllers [16]–[18]. In contrast, distributed ones are much preferable due to less communication burden and higher system scalability. However, most of the distributed controllers are parochially customized for either DC MGs or AC MGs [19]–[21]. A distributed control canonical form (DCCF), which can provide a generalized way for f_{ac} and V_{dc} restorations in the hybrid AC/DC MG, has not been reported. The deviated f_{ac} and V_{dc} straightforwardly indicate the loading conditions of AC and DC subgrids. Large f_{ac} and V_{dc} drops imply the heavy load and vice versa. The difference between f_{ac} and V_{dc} deviations helps to decide the transferred power of BIC so that the total MG loads can be appropriately shared by AC DGs and DC DGs. However, if f_{ac} and V_{dc} are tightly regulated and keep unchanged, the loading conditions of two subgrids are imperceptible. The lost loading information in the MG seriously challenge the normal operation of BIC, and this problem has also not been discussed so far.

To fill the aforesaid gaps, as well as retain the global system economic operation, in this paper, a distributed power control architecture is proposed for a hybrid AC/DC MG. The architecture consists of two levels. In the first level, the IC based droops are adopted in each subgrid to obtain the equalized ICs when the system reaches an equilibrium point. Nevertheless, only having droops will inevitably cause f_{ac} and V_{dc} fluctuations. Therefore, in the second level, a DCCF, which is uniformly applicable to both AC and DC subgrids, is proposed to concurrently restore f_{ac} and V_{dc}. Then, an original relative loading index (RLI) is proposed to uncover the hidden loading condition of each subgrid even if f_{ac} and V_{dc} are clamped as constants. By using RLI, the power reference of BIC can be conveniently defined, and the ICs of all DGs in the hybrid MG will converge to the same value in the steady state, which means the global system economic operation is accomplished. To examine the impacts of communication time delay on the system performances, a small signal model of the MG under the proposed architecture is derived. By analyzing the eigenvalue loci, it will be shown that the longer time delay results in larger transient oscillations and even destabilize the MG.

Following the introduction in Section I, the IC based droop schemes utilized in the first level are explained in Section II. Section III elaborates the proposed DCCF and the novel RLI. The control diagram of BIC is then meticulously illustrated based on RLI, and the effects of communication time delay on the MG stability are also explored. In Section IV and V, simulations together with hardware in loop (HIL) tests validate the feasibility and effectiveness of the proposed control architecture. Finally, conclusions are drawn in Section VI.

II. IC Based Droops in the First Level

A. System Description

A generic schematic of an autonomous hybrid AC/DC MG is shown in Fig. 1. RESs, such as photovoltaic (PV) panels and wind turbines (WTs), are operated in maximum power point tracking (MPPT) modes. DGs including diesel generators and microturbines would inherently induce operation costs due to the fuel consumption. Resistive loads (RLs) can be directly connected to AC and DC buses with no interfacing devices. Motor drives (MDs) are generally modeled as constant power loads (CPLs) because of their tightly regulated consumed power. The BIC bridges the AC and DC buses and enables the proper power interactions between the two subgrids.

Since the proposed control architecture aims to save the total operation costs, only DGs that bring costs will be considered in this paper. The simplified layouts of the studied subsystems are displayed in Fig. 2. In each subgrid, RESs, CPLs and RLs are combined as the lumped load (P_L),

$$P_{Ll} = P_{CPLsl} + P_{RLsl} - P_{RESsl} \tag{1}$$

where l denotes either ac or dc.

B. Economic Operation Problem

In the conventional power system, the cost (C_k) of a particular DG is usually related to its output power (P_k). This relation can be described by a quadratic function [22],

$$C_k = 0.5a_kP_k^2 + b_kP_k + c_k \tag{2}$$

where a_k, b_k, and c_k are the cost coefficients of the kth DG.

The economic operation model can be formulated below,

$$\begin{cases} \min C_{total} = \sum\limits_k C_k \\ s.t.\ P_{k,\min} \le P_k \le P_{k,\max}, P_{load} = \sum\limits_k^n P_k. \end{cases} \tag{3}$$

If P_k is confined within the permitted range, the necessary condition for total cost minimization is that the incremental costs (ICs) of all DGs are equal to some undetermined value λ [22],

$$IC_k = \lambda = \frac{\partial C_k}{\partial P_k} = a_kP_k + b_k. \tag{4}$$

Moreover, it is worth mentioning that once P_k reaches the predefined $P_{k,\min}$ or $P_{k,\max}$, the output power of the kth DG is limited to the bounded value. The remaining DGs continue to operate according to the above economic dispatch rules.

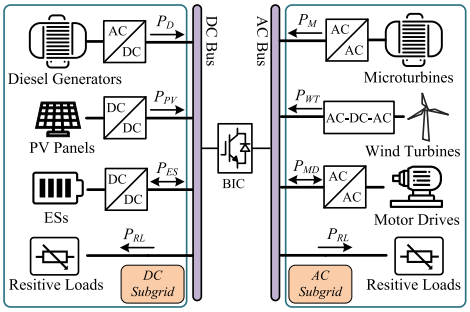

Fig. 1. A generic schematic of an autonomous hybrid AC/DC MG.

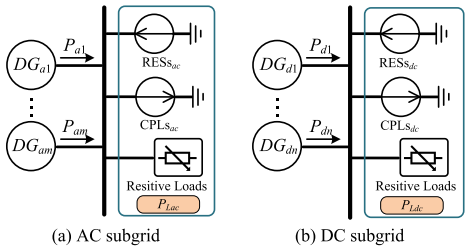

Fig. 2. Simplified schematics of AC subgrid and DC subgrid.

C. IC Based Droop in AC and DC Subgrids

In traditional droop schemes, the active power supplied by the DGs in AC and DC subgrids are proportional to their respective power ratings when f_{ac} and V_{dc} are synchronized. The droop principle can also be applied to the reactive power sharing, but normally accompanied by errors. The errors are caused by mismatched line impedances and system parameters. Although some methods for improving reactive power sharing accuracy could be found in [23] and [24], these amendments would not be discussed here as the reactive power only exists in AC subgrid and does not incur any cost [15], [25]. By properly relating the IC to f_{ac} and V_{dc}, the DG ICs can reach equality when f_{ac} and V_{dc} converge to certain values after system transition [14], [15]. This fact gives the IC based droops,

$$f_{ac} = f_{ac\max} - d_{ac} IC_i, IC_i = a_i P_i^M + b_i,\ \ i \in [1, m], \quad (5)$$

$$V_{dc} = V_{dc\max} - d_{dc} IC_j, IC_j = a_j P_j^M + b_j,\ \ j \in [1, n], \quad (6)$$

where $f_{ac\max}$ and $V_{dc\max}$ are the maximum AC frequency and DC bus voltage. d_{ac} and d_{dc} are the droop coefficients written as,

$$d_{ac} = f_{ac\max} - f_{ac\min}, d_{dc} = V_{dc\max} - V_{dc\min}. \quad (7)$$

It should be noted that the calculations of d_{ac} and d_{dc} are only related to the maximum deviations of f_{ac} and V_{dc}. A single droop controller does not need any information from others, which enhances the system applicability and scalability.

In (5) and (6), P_i^M and P_j^M are the measured power processed by the first order low pass filters (LPFs). Their dynamics are,

$$\tau_{ac}\dot{P}_i^M + P_i^M = P_i, \tau_{dc}\dot{P}_j^M + P_j^M = P_j, \quad (8)$$

where $\boldsymbol{\tau}_{ac}$ and τ_{dc} are the time constants of LPFs. P_i and P_j are the real-time active powers. For the AC subgrid, the ICs of all AC DGs are enforced to be identical with the synchronization of f_{ac},

$$IC_1 = \ldots = IC_i = \ldots = IC_m. \quad (9)$$

Similarly, in the DC subgrid, ICs are the same in steady state,

$$IC_1 = \ldots = IC_j = \ldots = IC_n. \quad (10)$$

From (5) to (10), it has been revealed that the IC based droops are naturally decentralized and the optimal operating point can be achieved with no communication. To reserve this advantage, the IC based droops are employed in the first level of the proposed control architecture. To eliminate the f_{ac} and V_{dc} deviations caused by droops, in the second level, a DCCF is proposed as a generalized method to concurrently restore f_{ac} and V_{dc} for the hybrid MG. The schematic of the proposed architecture is displayed in Fig. 3. Comprehensive explanations and relevant analyses will be conducted in the next section.

III. Distributed Control in the Second Level

Before proceeding to present the proposed DCCF, some preliminaries concerning graph theory should be introduced briefly for better understanding the relevant reasoning.

A. Graph Theory

Inside a communication graph [26], there are totally N nodes $\mathcal{V} = \{v_1, v_2, \ldots, v_N\}$, and $\varepsilon \subseteq \mathcal{V} \times \mathcal{V}$ denotes the set of edges connecting two different nodes. The set of neighbors of the yth node can be written as $\mathcal{N}_y \triangleq \{v_z \subseteq \mathcal{V} : (y, z) \subseteq \varepsilon\}$. Adjacency matrix $\boldsymbol{\mathcal{A}} \subseteq \mathbb{R}^{N\times N}$ has elements $a_{yz} = a_{zy} = 1$ if $v_z \subseteq \mathcal{N}_y$, otherwise, $a_{yz} = a_{zy} = 0$. This means that if node z is one of the neighbors of node y, then node z can receive information from node y, and vice versa. The in-degree matrix is denoted as $\boldsymbol{\mathcal{D}} = diag\{d_y\} \subseteq \mathbb{R}^{N\times N}$, where $d_y = \sum a_{yz}$ if $v_z \subseteq \mathcal{N}_y$. Laplacian matrix of the graph can be then defined as $\boldsymbol{L} = \boldsymbol{\mathcal{A}} - \boldsymbol{\mathcal{D}}$ which also belongs to $\mathbb{R}^{N\times N}$. It is worth mentioning that the correct functioning of the hybrid MG can be guaranteed if the communication graph maintains at least a spanning tree [19]. Concretely, in each subgrid, there exists at least one DG such that the information of that DG can be propagated to all other DGs. This DG, in this paper, is defined as the leader, whereas the other DGs are defined as the followers.

B. The Proposed DCCF

1) Control Objectives: In Section II, it is easy to know that the output power of a particular DG is finally regulated to reach a level such that all DG ICs in a particular subgrid are the same. An exemplification has been shown in Fig. 4. For convenient explanation, f_{ac} and V_{dc} are uniformly represented as x. The rudimentary IC based droop curve is given by the red solid line 1. At the beginning, DG_a and DG_b have the common IC_1 with x_0, and the corresponding powers are P_{a1} and P_{b1}. To regulate x to its nominal value x_n, the compensating variable Δx is generated and the newly obtained droop curve could be described by the red solid line 2. As a result, the

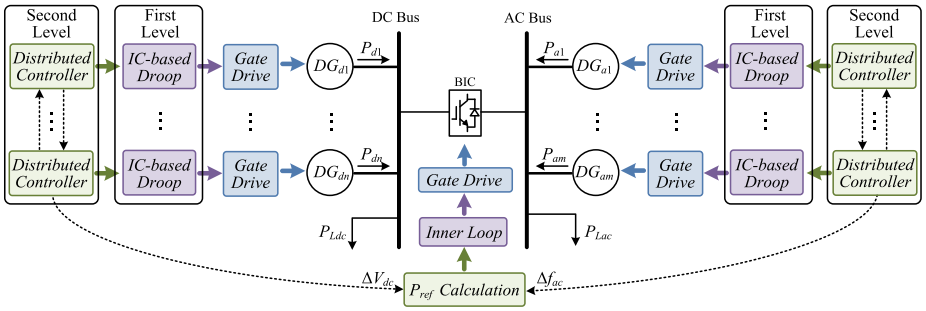

Fig. 3. The proposed distributed control architecture for a representative hybrid AC/DC MG.

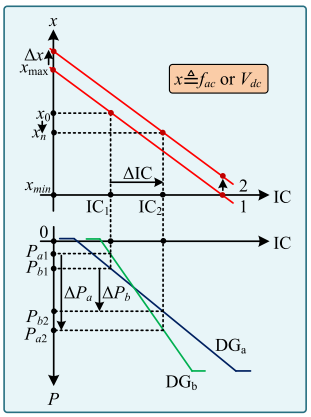

Fig. 4. System droop characteristics with f_{ac}/V_{dc} restoration.

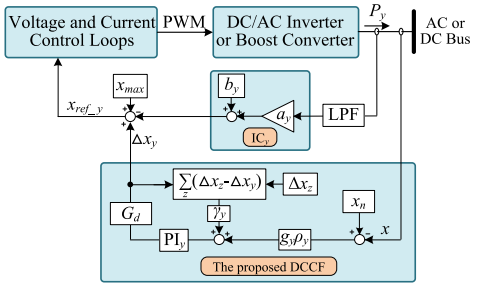

Fig. 5. Control diagram of the proposed DCCF.

system functions at a new steady point where the DG ICs are equalized at IC_2, and DG_a supplies P_{a2} and DG_b supplies P_{b2}.

It is essential to stress that in the first level, the economic operation can be accomplished only when all DGs utilize the identical droop equations. This mechanism should also be maintained even after f_{ac} and V_{dc} restorations. In other word, in each subgrid, the compensating variables used for revising the rudimentary droop functions have to be the same, which formulates the first control objective for the DCCF,

$$\Delta x_y = \Delta x_z, \ \forall y, z \in i \ or \ j. \tag{11}$$

On the other hand, to largely reduce the communication complexity and enhance the system scalability, the proposed controller in the second level should be completely distributed. Hence, in addition to constraint (11), another requirement is that the information of f_{ac} or V_{dc} would only be known by the leader DG in a subgrid. The follower DGs are scheduled to achieve consensus with the leader one by merely using the information obtained from their neighbors. In the case that the leader DG are accidentally down, its leading role can be randomly assigned to any of the rest DGs for ensuring the system normal operation, and in this way, the PnP capability can also be reinforced.

2) The Proposed DCCF: Responding to the above two goals, a DCCF is proposed for the DG numbered by "y" as in (12),

$$\begin{cases} \Delta x_y = G_d\left(k_{py}e_y + k_{iy}\int e_y dt\right) \\ e_y = \gamma_y \sum_z \left(\Delta x_z - \Delta x_y\right) + g_y\rho_y(x_n - x) \end{cases}, \tag{12}$$

where γ_y, $\rho_y \subseteq \mathbb{R}^+$ are the proportional gains. g_y is the pinning gain which is nonzero for the leader DG. e_y is the summed error which is processed by the proportional-integral (PI) controller. e_y will be finally forced to be zero at the end of system transition due to the PI regulation. As observed from (12), e_y consists of two types of errors, $\Delta x_z - \Delta x_y$ and x_n-x respectively. The former represents the difference between the localized compensating signal and the signal produced by the neighbors of DG_y. This error is to ensure that the control objective (11) can be achieved. The latter error denotes the deviation of f_{ac} or V_{dc}. The presence of this term aims to enforce the real time AC frequency and DC bus voltage to track their respective nominal values.

The control diagram of the proposed DCCF and its cooperation with IC based droop are displayed in Fig. 5. As the information exchange processes are involved in DCCF, the communication time delay will be inevitably induced. For precise modeling, the delay term $G_d = 1/(\tau_d s + 1)$ is embodied in the first equation of (12). τ_d is the time delay which will be shown to potentially impair system stability.

C. The Proposed RLI and Control Strategy of BIC

1) The Proposed RLI: In AC and DC subgrids, the fluctuated x directly indicates the loading conditions. With the adoption of normalization scheme, and properly scheduling the transferred power of BIC, the global load balancing of the entire hybrid MG can be achieved [27]. However, due to the existence of DCCF, f_{ac} and V_{dc} are strictly clamped at their nominal values. The consequent problem is that the loading situations of the two subgrids are no longer accessible. Existing control methods of BIC in [27] and [28] will absolutely fail.

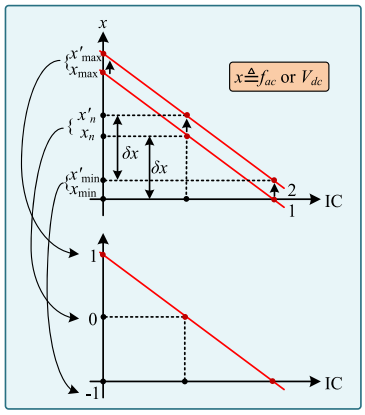

Fig. 6. Relative loading index calculation.

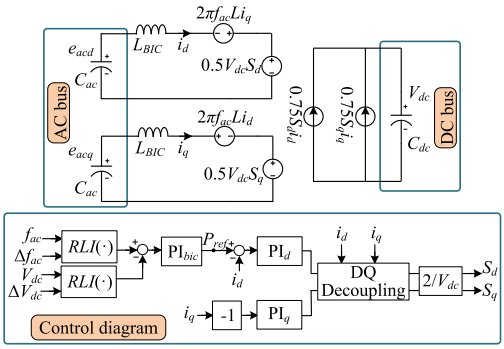

Fig. 7. Modeling of BIC and its control diagram.

To tackle this issue, an original RLI is proposed in this paper to extract the hidden loading information after f_{ac}/V_{dc} recovery,

$$\mathrm{RLI}(x) = \frac{x - x'_n}{\delta x}, x'_n = x_n + \Delta x, \tag{13}$$

where $x_n = 0.5(x_{\max} + x_{\min})$ is the nominal value. $\delta x = 0.5(x_{\max} - x_{\min})$ is a constant denoting the maximum deviation of x from x_n. As emphasized in Fig. 4, the DCCF enables the droop curve to shift upward by Δx to simultaneously realize IC equalization and f_{ac}/V_{dc} restoration. The main idea of RLI is to obtain the superposed term Δx by the communication link and remove it from the numerator of (13). By doing this, as seen from Fig. 6, x can be accordingly mapped into the range of $[-1, 1]$, which is similar to the normalization scheme documented in [27] and [28]. By means of RLI, even though f_{ac} and V_{dc} are rigorously regulated, the loading status of each subgrid can be accurately calculated, thus facilitating the proper control of BIC.

2) Control of BIC: For a given hybrid MG, BIC should be scheduled to make sure that the RLIs of AC and DC subgrids are the same. As a result, the ICs equalization of all DGs in the MG can be realized. Mathematical modeling of BIC in rotating frame and the control diagram are shown in Fig. 7 where the reference direction of power flow is also clearly defined. The difference of RLI(f_{ac}) and RLI(V_{dc}) is processed by a PI controller which further generates the active power reference for BIC. If RLI(f_{ac}) > RLI(V_{dc}), which means the AC subgrid is lightly loaded while the DC subgrid suffers from heavy load, then BIC drives the power flowing from the AC subgrid to the DC one. Inversely, the power of the DC subgrid would be channeled to the AC one in the case of RLI(f_{ac}) < RLI(V_{dc}). Because of the PI regulation, the RLI discrepancy can be eliminated in system steady state. Additionally, the power reference in q axis is con ured as zero as there is no reactive power in DC network.

Inserting compensating values generated by (12) into (5) and (6), droop equations should be revised accordingly,

$$f_{ac} = f_{ac\max} - d_{ac}IC_i + \Delta f_{ac}, \tag{14}$$

$$V_{dc} = V_{dc\max} - d_{dc}IC_j + \Delta V_{dc}. \tag{15}$$

Applying RLI calculation rule to (14) and (15) yields,

$$\mathrm{RLI}(f_{ac}) = \frac{f_{ac\max} - d_{ac}IC_i + \Delta f_{ac} - (f_{acn} + \Delta f_{ac})}{0.5(f_{ac\max} - f_{ac\min})}, \tag{16}$$

$$\mathrm{RLI}(V_{dc}) = \frac{V_{dc\max} - d_{dc}IC_j + \Delta V_{dc} - (V_{dcn} + \Delta V_{dc})}{0.5(V_{dc\max} - V_{dc\min})}. \tag{17}$$

Equating RLI(f_{ac}) and RLI(V_{dc}) gives the following,

$$\mathrm{RLI}(f_{ac}) = \mathrm{RLI}(V_{dc}) \Rightarrow IC_i = IC_j. \tag{18}$$

Since subscripts i and j represent arbitrary DGs in AC and DC subgrids, thus the complete form of (18) can be written below,

$$\begin{aligned} IC_1 = \ldots = IC_i = \ldots = IC_m \\ = IC_1 = \ldots = IC_j = \ldots = IC_n. \end{aligned} \tag{19}$$

As seen from (19), by properly scheduling the BIC power to equalize the RLIs of the two subgrids, all DG ICs converge to the same value in steady state. This means the total operating cost can be minimized and the global system economic operation of the hybrid AC/DC MG is realized. When the output power of a certain DG reaches its predefined value, the compensating signals produced by the DCCFs will spontaneously achieve a new equilibrium such that the rest DGs are working in economic dispatch principle and f_{ac}/V_{dc} restorations can be realized. Observing from (13), it is worth noting that the RLI calculations only involve f_{ac}, V_{dc}, Δf_{ac} and ΔV_{dc}. The BIC does not necessarily know the exact DG ICs. Considering a saturated DG in AC or DC subgrid, the DG delivers the bounded power and stops short of responding to the compensation signal. Yet its distributed controller keeps staying in the subgrid communication network and maintains synchronization with other DGs. Once the power saturation terminates, the compensating signal is again imposed in the DG inner loop so that this DG can participate in the f_{ac} or V_{dc} regulations. Thus, the saturated DG would not influence RLI computations and the BIC control diagram consistently stands.

D. Communication Time Delay Stability Analysis

The above contexts comprehensively explain the equilibrium operating point of the hybrid MG under the proposed distributed control architecture. As mentioned earlier, the distributed control requires DGs to exchange information through

communication networks, which unavoidably results in communication time delay. The large time delay in the MG may compromise the system convergence speed, and even cause system oscillations [29]. Therefore, it is necessary to analyze the impacts of communication time delay on overall performances of the hybrid AC/DC MG. To do that, two considerations have to be made. Firstly, as detailed in Fig. 4, it is fairly possible for a particular DG to have the IC locating beyond the linear range of the droop curve. This means the output power of the DG has reached the minimum or maximum value. In this situation, the DG keep delivering the bounded power and the other DGs still operate abiding by the economic dispatch rules. However, in this paper, this exceptional scenario would be excluded from stability studies since those DGs working with the bounded power intrinsically act as constant power sources (CPSs) which contribute the widened stability margin to the MG [30]. Secondly, as understood from [25], only the IC based droop characteristics and the dynamics of the proposed DCCF are considered because they are the two major factors that may undermine the MG stability.

Substituting (8) into (14) and (15), the resulted compact forms can be written as below,

$$\begin{cases} \boldsymbol{\tau}_{ac}\dot{\boldsymbol{f}} = f_{ac\max}\mathbf{1}_m - \boldsymbol{f} - d_{ac}\boldsymbol{a}_{ac}\boldsymbol{P}_{ac}\mathbf{1}_m - d_{ac}\boldsymbol{b}_{ac} + \Delta\boldsymbol{f} \\ \boldsymbol{\tau}_{dc}\dot{\boldsymbol{V}} = V_{dc\max}\mathbf{1}_n - \boldsymbol{V} - d_{dc}\boldsymbol{a}_{dc}\boldsymbol{P}_{dc}\mathbf{1}_n - d_{dc}\boldsymbol{b}_{dc} + \Delta\boldsymbol{V} \end{cases} \tag{20}$$

where

$$\begin{aligned} &\boldsymbol{f} = [f_1 \cdots f_i \cdots f_m]^T, \boldsymbol{V} = [V_1 \cdots V_j \cdots V_n]^T, \\ &\Delta\boldsymbol{f} = \left[\Delta f_{ac1} \cdots \Delta f_{aci} \cdots \Delta f_{acm}\right]^T, \\ &\Delta\boldsymbol{V} = \left[\Delta V_{dc1} \cdots \Delta V_{dcj} \cdots \Delta V_{dcn}\right]^T, \\ &\boldsymbol{b}_{ac} = [b_1 \cdots b_i \cdots b_m]^T, \boldsymbol{b}_{dc} = \left[b_1 \cdots b_j \cdots b_n\right]^T, \\ &\boldsymbol{a}_{ac} = \mathrm{diag}(a_1 \cdots a_i \cdots a_m), \boldsymbol{a}_{dc} = \mathrm{diag}\left(a_1 \cdots a_j \cdots a_n\right), \\ &\boldsymbol{P}_{ac} = \mathrm{diag}(P_1 \cdots P_i \cdots P_m), \\ &\boldsymbol{P}_{dc} = \mathrm{diag}\left(P_1 \cdots P_j \cdots P_n\right), \boldsymbol{\tau}_{ac} = \mathrm{diag}(\tau_{ac1} \cdots \tau_{aci} \cdots \tau_{acm}), \\ &\boldsymbol{\tau}_{dc} = \mathrm{diag}\left(\tau_{dc1} \cdots \tau_{dcj} \cdots \tau_{dcn}\right), \end{aligned}$$

$\mathbf{1}_m$ and $\mathbf{1}_n$ are column vectors with all elements being 1.

Replacing x in (12) with f_{ac} and V_{dc} respectively, the compact forms of controllers can also be obtained,

$$\begin{cases} \boldsymbol{\tau}_{dac}\Delta\dot{\boldsymbol{f}} = \boldsymbol{k}_{pac}\boldsymbol{e}_{ac} + \boldsymbol{k}_{iac}\boldsymbol{\psi}_{ac} - \Delta\boldsymbol{f}, \dot{\boldsymbol{\psi}}_{ac} = \boldsymbol{e}_{ac} \\ \boldsymbol{\tau}_{ddc}\Delta\dot{\boldsymbol{V}} = \boldsymbol{k}_{pdc}\boldsymbol{e}_{dc} + \boldsymbol{k}_{idc}\boldsymbol{\psi}_{dc} - \Delta\boldsymbol{V}, \dot{\boldsymbol{\psi}}_{dc} = \boldsymbol{e}_{dc} \end{cases}, \tag{21}$$

where

$$\begin{aligned} &\boldsymbol{k}_{pac} = \mathrm{diag}(k_{p1} \cdots k_{pi} \cdots k_{pm}), \\ &\boldsymbol{k}_{pdc} = \mathrm{diag}(k_{p1} \cdots k_{pj} \cdots k_{pn}), \\ &\boldsymbol{k}_{iac} = \mathrm{diag}(k_{i1} \cdots k_{ii} \cdots k_{im}), \ \boldsymbol{k}_{idc} = \mathrm{diag}(k_{i1} \cdots k_{ij} \cdots k_{in}), \\ &\boldsymbol{\tau}_{dac} = \mathrm{diag}(\tau_{d1} \cdots \tau_{di} \cdots \tau_{dm}), \\ &\boldsymbol{\tau}_{ddc} = \mathrm{diag}(\tau_{d1} \cdots \tau_{dj} \cdots \tau_{dn}), \end{aligned}$$

$\boldsymbol{\psi}_{ac}$ and $\boldsymbol{\psi}_{dc}$ are the intermediate state variables induced by integrators in (12). $\boldsymbol{e}_{ac}$ and $\boldsymbol{e}_{dc}$ are the error vectors,

$$\begin{cases} \boldsymbol{e}_{ac} = -\boldsymbol{\gamma}_{ac}\boldsymbol{L}_{ac}\Delta\boldsymbol{f} + \boldsymbol{G}_{ac}\boldsymbol{\rho}_{ac}\left(f_{acn}\mathbf{1}_m - \boldsymbol{f}\right) \\ \boldsymbol{e}_{dc} = -\boldsymbol{\gamma}_{dc}\boldsymbol{L}_{dc}\Delta\boldsymbol{V} + \boldsymbol{G}_{dc}\boldsymbol{\rho}_{dc}(V_{dcn}\mathbf{1}_n - \boldsymbol{V}) \end{cases}, \tag{22}$$

where

$$\begin{aligned} &\boldsymbol{\gamma}_{ac} = \mathrm{diag}(\gamma_1 \cdots \gamma_i \cdots \gamma_m), \ \boldsymbol{\gamma}_{dc} = \mathrm{diag}(\gamma_1 \cdots \gamma_j \cdots \gamma_n), \\ &\boldsymbol{G}_{ac} = \mathrm{diag}(g_1 \cdots g_i \cdots g_m), \ \boldsymbol{G}_{dc} = \mathrm{diag}(g_1 \cdots g_j \cdots g_n), \\ &\boldsymbol{\rho}_{ac} = \mathrm{diag}(\rho_1 \cdots \rho_i \cdots \rho_m), \ \boldsymbol{\rho}_{dc} = \mathrm{diag}(\rho_1 \cdots \rho_j \cdots \rho_n), \end{aligned}$$

$\boldsymbol{I}_{m\times m}$ and $\boldsymbol{I}_{n\times n}$ are the identity matrices. $\boldsymbol{L}_{ac}$ and $\boldsymbol{L}_{dc}$ are the Laplacian matrices describing communication networks of AC and DC subgrids. f_{acn} and V_{dcn} are the nominal AC frequency and nominal DC bus voltage respectively.

Combining (20), (21) and (22), and performing small signal disturbances, the dynamic model can be derived below,

$$\begin{bmatrix} \dot{\tilde{\boldsymbol{f}}} \\ \dot{\tilde{\boldsymbol{V}}} \\ \Delta\dot{\tilde{\boldsymbol{f}}} \\ \Delta\dot{\tilde{\boldsymbol{V}}} \\ \dot{\tilde{\boldsymbol{\psi}}}_{ac} \\ \dot{\tilde{\boldsymbol{\psi}}}_{dc} \end{bmatrix} = \begin{bmatrix} -\boldsymbol{\tau}_{ac}^{-1} & \mathbf{0} & \boldsymbol{\tau}_{ac}^{-1} & \mathbf{0} & \mathbf{0} & \mathbf{0} \\ \mathbf{0} & -\boldsymbol{\tau}_{dc}^{-1} & \mathbf{0} & \boldsymbol{\tau}_{dc}^{-1} & \mathbf{0} & \mathbf{0} \\ \boldsymbol{a_1}\boldsymbol{A}_1 & \mathbf{0} & \boldsymbol{C}_1 & \mathbf{0} & \boldsymbol{b_1} & \mathbf{0} \\ \mathbf{0} & \boldsymbol{a}_2\boldsymbol{A}_2 & \mathbf{0} & \boldsymbol{C}_2 & \mathbf{0} & \boldsymbol{b}_2 \\ \boldsymbol{A}_1 & \mathbf{0} & \boldsymbol{B}_1 & \mathbf{0} & \mathbf{0} & \mathbf{0} \\ \mathbf{0} & \boldsymbol{A}_2 & \mathbf{0} & \boldsymbol{B}_2 & \mathbf{0} & \mathbf{0} \end{bmatrix} \times \begin{bmatrix} \tilde{\boldsymbol{f}} \\ \tilde{\boldsymbol{V}} \\ \Delta\tilde{\boldsymbol{f}} \\ \Delta\tilde{\boldsymbol{V}} \\ \tilde{\boldsymbol{\psi}}_{ac} \\ \tilde{\boldsymbol{\psi}}_{dc} \end{bmatrix}, \tag{23}$$

where

$$\begin{aligned} &\boldsymbol{A}_1 = -\boldsymbol{G_{ac}}\boldsymbol{\rho_{ac}}, \ \boldsymbol{B}_1 = -\boldsymbol{\gamma}_{ac}\boldsymbol{L}_{ac}, \ \boldsymbol{A}_2 = -\boldsymbol{G_{dc}}\boldsymbol{\rho_{dc}}, \\ &\boldsymbol{B}_2 = -\boldsymbol{\gamma}_{dc}\boldsymbol{L}_{dc}, \ \boldsymbol{a}_1 = \boldsymbol{\tau}_{dac}^{-1}\boldsymbol{k}_{pac}, \ \boldsymbol{b}_1 = \boldsymbol{\tau}_{dac}^{-1}\boldsymbol{k}_{iac}, \\ &\boldsymbol{a}_2 = \boldsymbol{\tau}_{ddc}^{-1}\boldsymbol{k}_{pdc}, \\ &\boldsymbol{b}_2 = \boldsymbol{\tau}_{ddc}^{-1}\boldsymbol{k}_{idc}, \ \boldsymbol{C}_1 = \boldsymbol{a}_1\boldsymbol{B}_1 - \boldsymbol{\tau}_{dac}^{-1}\boldsymbol{I}_{m\times m}, \\ &\boldsymbol{C}_2 = \boldsymbol{a}_2\boldsymbol{B}_2 - \boldsymbol{\tau}_{ddc}^{-1}\boldsymbol{I}_{n\times n}. \end{aligned}$$

Noting that (23) gives a generalized form of the system model, for simplicity, a scenario that each subgrid has 2 DGs (i.e., $m = n = 2$) is considered. It is further assumed that the capacities of the two subgrids are comparable, and the hybrid MG has the symmetrical structure [27]. This allows setting the PI parameters of DCCF in both subgrids to be identical, i.e., $\boldsymbol{k}_{pac} = \boldsymbol{k}_{pdc} = k_p\boldsymbol{I}_{2\times2}$, $\boldsymbol{k}_{iac} = \boldsymbol{k}_{idc} = k_i\boldsymbol{I}_{2\times2}$, where k_p and k_i are constants. Besides, AC and DC subgrids have the identical communication networks, hence, the delay matrices in (21) can also be equally set, i.e., $\boldsymbol{\tau}_{dac} = \boldsymbol{\tau}_{ddc} = \tau_d\boldsymbol{I}_{2\times2}$.

Fig. 8 shows that the dominant eigenvalue behaviors of the autonomous system described by (23) with τ_d increasing from 0.05s to 1.15s. The remaining eigenvalues that have the real parts less than -8 are neglected. In the case of $\tau_d = 0.5$s, complex eigenvalues are $-2.1 \pm j31.2$ which are in left half plane and the MG system is stable. The oscillation frequency pertaining to these eigenvalues is estimated as 5Hz. In contrast, the MG system is unstable when communication time delay increases to 1s. The corresponding eigenvalues are $0.15 \pm j22.1$ which have the oscillation frequency of 3.5Hz. Observed from Fig. 8, for the hybridized system under study, the maximum communication time delay should be smaller

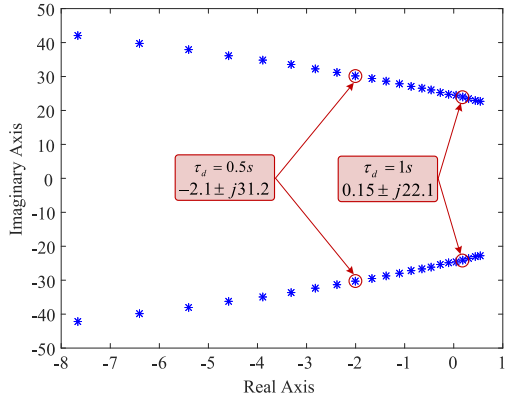

Fig. 8. Root loci plot with τ_d variation.

than 0.9s in order to attain the stable operation. All conclusions discussed above will be verified y.

E. Discussions

1) Decoupling of the Two Control Levels: There are two ways to avoid the system instability caused by the interactions between the two control levels. Firstly, for a particular DG in either AC or DC subgrid, the dynamics of its inner control loops in the first level should be tuned much faster than that of DCCF in the second level. By doing so, the signals generated by the DCCF can be viewed as a constant for the inner loops, and the two control levels can be completely decoupled. Secondly, when the hybrid MG system is started, it is highly recommended to enable the DCCF only after the first level controllers function stably. Therefore, the underlying stability incurred by the interactions of the two levels can be subtly circumvented from the perspective of operating procedures.

2) The Control of Energy Storages: Energy storages (ESs) are important in the MG system. In this paper, ESs would not be involved in economic dispatch problems. Due to the absence of the main grid, the autonomous hybrid MG may have low system inertia. It is reasonable to schedule ESs as the system energy backup. In AC and DC subgrids, for the worst case that all DGs are down, ESs could be utilized to build up AC or DC bus, and supply the requested power to critical loads. For a less serious case that the system RLI goes beyond the predefined range, ESs should work in power control mode to limit RLI in $[-1, 1]$. For instance, when the RES generations exceed the power consumptions, RLI tends to exceed 1 due to the surplus power. Upon this loading condition, ESs would absorb power from the MG and regulate RLI to be slightly less than 1 or clamped at 1. Conversely, assuming that the MG is heavily loaded, RLI may drop below -1. ESs would release power so that RLI can increase to a bit larger than -1 or bounded at -1, thus ensuring the safe MG operations.

3) The Impacts of Non-Inductive or Complex Line Impedances: In high voltage power systems, the transmission lines can be considered to be inductive. However, the line impedances of low voltage MGs would be non-inductive or complex. The active power regulations may affect the reactive power variations and vice versa. To retrieve the decoupled features of active and reactive powers, virtual impedance techniques in [31] can be utilized to shape the DG output impedances to be purely inductive. The proposed method can thus be applied to the system of non-inductive or complex impedances without any revision. Furthermore, as indicated by (14), the active power distribution is only related to frequency fluctuations. There is only one common frequency prevailing in the AC subgrid in the steady state, which ensures the nearly exact active load sharing among DGs. Hence, ICs equalization merely depends on the AC frequency. The impacts of line impedances on the ICs are minor and could be neglected.

4) The Motivation for Configuring Leader DGs: In both AC and DC subgrids, it is true that the convergence speed of the DCCF could be faster provided that all DGs know x_n. However, this unnecessarily requires DGs to have more prior knowledge of a given system, which may sacrifice the MG flexibility and PnP property. In this paper, the worst case that only leader DG knows the information of x_n is considered. Then a follower DG with the DCCF only need to establish the communications with its neighbors, and system consensus could be achieved autonomously. Besides, it is worth noting that there are two control levels in the proposed distributed control architecture, i.e., IC based droop in the first level and the DCCF in the second level. The dynamic of the second level should be strictly slower than that of the first level to avoid dynamic conflicts between the two levels. In this sense, the convergence of the DCCF should not be over rapid, and hence, the scenario that all DGs know x_n would not be encouraged.

5) Advantages of the Proposed Scheme Over Existing Methods: In the published studies, the central idea of distributed optimization is to choose DG ICs as consensus variables and drive them to be the same. A distributed consensus based approach in [32] assigns each DG in a grid with an agent which produces the power reference for the DG. Those agents have to locally estimate the mismatch between demands and total generations. However, the estimated mismatch may not equal the real one, which possibly undermines the ICs equalization. The similar challenge can also be found in [33] where highly accurate predictions of RES generations and load variations are compulsory. Considering the random wind power, the economic dispatch for smart grids is studied in [34]. An initialization scheme has to be repeatedly exerted at each instant of wind power change, which may not be practical in real applications. A distributed algorithm reported in [35] requires that the output powers of all DGs have to be collected and sent to a particular DG. Yet the requirements of this algorithm are identical to that in central controls, which inevitably compromises the system flexibility and scalability. Although the method proposed in [36] achieves ICs consistence with avoiding load power forecasting, the method unnecessarily escalates the computational burdens by introducing a mode switching control and intentionally reducing the consensus speed when the output power of a DG reaches the bounded value.

Compared with the above distributed optimization methods, the proposed architecture has the following advantages.

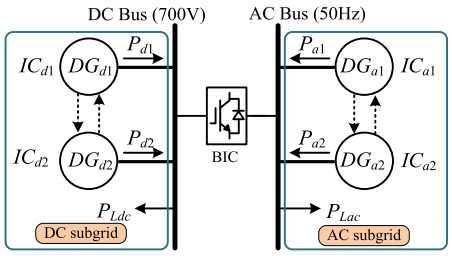

Fig. 9. The representative hybrid AC/DC MG.

Firstly, f_{ac}/V_{dc} can be perfectly stabilized at their nominal values, which will certainly protect those f_{ac}-/V_{dc}-sensitive loads and significantly improve system power qualities. Secondly, no prediction of RESs and loads would be needed. The power balancing between the generation and the consumption can be autonomously achieved in the studied hybrid MG. Thirdly, when the output power of a DG is saturated, without any mode transition or changing control schemes, the proposed architecture allows the rest DGs continuing to share the load based on economic dispatch principle. Fourthly, the existing distributed optimizations share the drawback that they are provincially tailored for AC MG or DC MG. But in the hybrid MG, AC and DC subgrids coexist. The power management may involve more challenges, which motivates the proposition of RLI. By configuring the BIC to equate subgrid RLIs, the ICs of all DGs in the MG can be equalized, and hence, the global system economic operation can be accomplished.

IV. Simulations

A. Comparisons of Classical Droop and IC Based Droop

Fig. 9 shows a representative hybrid MG structure for meticulous comparisons of system dynamics with conventional droops and the IC based droops. Relevant system parameters are summarized in TABLE I and TABLE II. The Laplacian matrices depicting communication graphs of the two subgrids can be written as $\boldsymbol{L}_{ac} = \boldsymbol{L}_{dc} = [1\ -1; -1\ 1;]$. For a subgrid, unlike the centralized control where a central controller has to send commands to all DGs, the proposed DCCF is fully distributed. As mentioned before, only the leader DG knows the information x_n. The follower DGs endeavor to achieve consensus with the leader one such that the distributed controllers of all DGs in the subgrid produce the identical compensating variables for first level controllers. For AC and DC subgrids in Fig. 9, leading roles are assigned to DG_{d1} and DG_{a1} respectively, whereas DG_{d2} and DG_{a2} are configured as the followers. On this basis, the pinning matrices in (22) can be derived as $\boldsymbol{G}_{ac} = \boldsymbol{G}_{dc} = [1\ 0;\ 0\ 0;]$.

Assuming the power rating of each DG is 15kW, for AC DGs (DG_{a1} and DG_{a2}), their classical droop gains are computed as 2/15000. By the same token, the droop coefficients of DG_{d1} and DG_{d2} are derived as 20/15000. According to (7), d_{ac} and d_{dc} could be calculated as 2 and 20, respectively. Observing from Fig. 10, for conventional droops, the summed load across the hybrid MG is around 24kW at the beginning. Due to the f_{ac} and V_{dc} regulation mechanisms of the DCCF, the frequency in AC subgrid and the bus voltage in DC subgrid keep unchanged at 50Hz and 700V. On the condition that load power steps up to 49kW, the total cost of the MG system increases from 18\$/h to 68.2\$/h. Then f_{ac} and V_{dc} are quickly recovered to their nominal values. For fair comparisons, the same loading profile is exerted in the MG when IC based droops are utilized. As shown in Fig. 11, initially, DG ICs are equalized at about 0.65\$/kWh. The frequency drop and the voltage drop are found at the instant of load step-up. Fortunately, the DG IC equalization maintains unaffected by the sudden load change, and all DG ICs rise to 1.35\$/kWh in the steady state. Comparing Fig. 10(e) and Fig. 11(e) indicates that the entire cost of DGs controlled by IC based droops is always less than the classical droops no matter how the loading condition varies.

TABLE I
System Parameters

Parameter	Description	Value
$f_{ac\max}$	Maximum AC frequency	51Hz
$V_{dc\max}$	Maximum DC bus voltage	710V
f_{acn}	Nominal AC frequency	50Hz
V_{dcn}	Nominal DC bus voltage	700V
τ_{ac}	LPF time constant	2πe-3
τ_{dc}	LPF time constant	2πe-3
τ_d	Communication time delay	20us
k_p	Proportional gain in DCCF	7
k_i	Integral gain in DCCF	800

TABLE II
Coefficients of Cost Functions in Fig. 9

	a_k	b_k	c_k
DG_{d1}	9.4e-2	1.22e-2	0.25
DG_{d2}	7.8e-2	3.41e-2	0.35
DG_{a1}	13e-2	5.9e-2	0.25
DG_{a2}	9.5e-2	8.5e-3	0.35

B. Hybrid MG With Unexpected DG Failures

Upon the hybrid MG system displayed in Fig. 9, simulation results for a scenario that DG_{a2} and DG_{d2} fail in sequence are shown in Fig. 12. Initially, AC frequency and DC bus voltage are perfectly stabilized at 50Hz and 700V under the proposed distributed control architecture. However, when DG_{a2} is unfortunately down at 1s, a significant frequency drop of 1Hz is observed, and a slight voltage deviation also occurs. For this situation, the DG_{a2} power immediately falls to zero. The ICs of DG_{d1}, DG_{d2}, DG_{a1} gradually rise to 1.1\$/kWh from 0.8\$/kWh. When DG_{d2} is unpredictably out of service at 4s, a drastic voltage drop of around 10V could be inspected, and a small frequency fluctuation takes place. Due to the mechanisms of the proposed control scheme, the ICs of DG_{a1} and DG_{d1} are still equalized at around 1.9\$/kWh. Therefore, it is easy to understand that the global system economic operation of the hybrid MG could be effectively realized even in the case of DG failures.

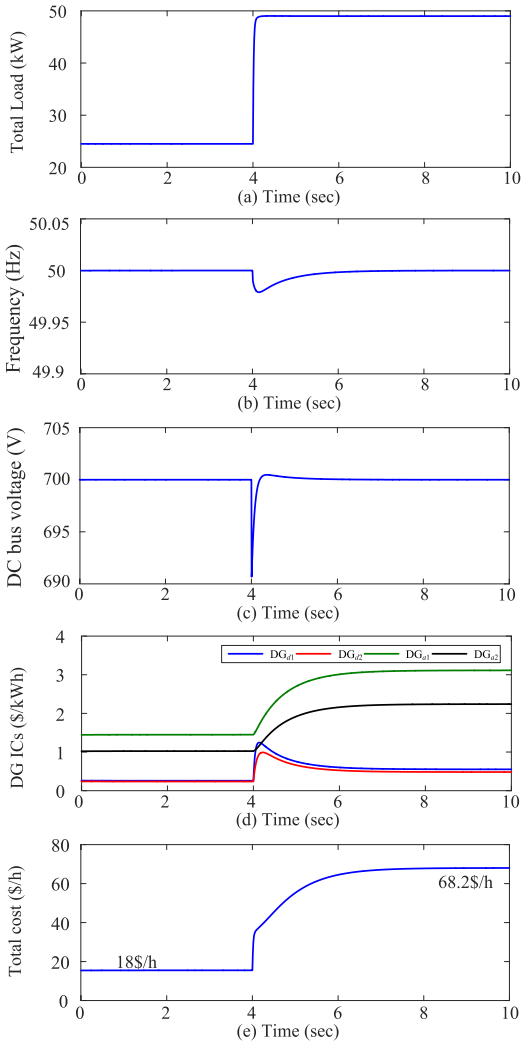

Fig. 10. The representative hybrid MG under conventional droops.

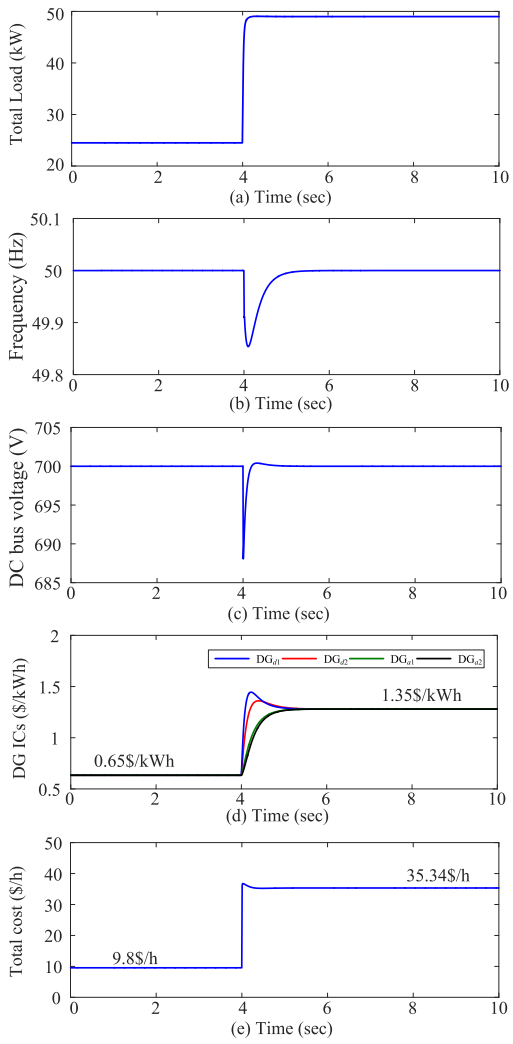

Fig. 11. The representative hybrid MG under IC based droops.

C. Applications to More Complex Hybrid Systems

Besides dealing with the representative system configuration shown in Fig. 9, the proposed distributed control architecture can also be generalized to complex hybrid systems, such as the multi-bus system (Fig. 13), the radially connected system (Fig. 15), the typical system with multiple DGs linking in parallel (Fig. 17).

1) The Multi-Bus System: In Fig. 13, the hybrid MG has a DC subgrid with three buses of different voltage levels (700V, 380V and 1000V). BIC_1 bridges DC bus_1 and AC bus (50Hz), whereas DC bus_2 and DC bus_3 are coupled to DC bus_1 though BIC_2 and BIC_3 respectively. The three BICs are in power control modes. All buses are separately integrated with two DGs which communicate with each other. P_{Ldc1}, P_{Ldc2}, P_{Ldc3}, and P_{Lac} represent local loads of the buses. Simulation results have been plotted in Fig. 14. At the beginning, all DG ICs can be read as 0.38$/kWh. The step-ups of P_{Ldc1}, P_{Ldc2}, P_{Ldc3}, and P_{Lac} are consecutively enabled at 2s, 5s, 8s and 11s, all ICs sequentially increase to 0.5$/kWh, 0.63$/kWh, 0.68$/kWh and 0.71$/kWh. The ICs equalization maintains unaffected by load fluctuations. The distributed control architecture enables to regulate each bus to their nominal values (700V, 380V, 1000V, 50Hz), which definitely enhances the system power quality.

2) The Radially Connected System: A radial MG can be recognized that each source inside the system is connected to at most two sources. A hybrid MG which incorporates an AC subgrid in radial connection and two DC subgrids is shown in Fig. 15. Three AC DGs individually control their local bus and each DC subgrid has two DGs. Similar to Fig. 7, the control objectives of BIC_1 and BIC_2 are to equalize RLIs of the three subgrids so that DG ICs could be consistent in the steady state. Fig. 16 shows the simulation results. At 2s, P_{Ldc1} is suddenly increased, the DG ICs rise from 0.34$/kWh to 0.50$/kWh. Afterward, P_{Ldc2} and P_{Lac} step up at 6s and 10s respectively, the ICs accordingly grow to 0.66$/kWh and 0.84$/kWh. DC bus voltages and AC frequency are stabilized at 700V and 50Hz due to the proper functioning of the DCCFs. With the proposed control method, the global system economic operation could be effectively accomplished.

3) The Typical System With Multiple DGs Linking in Parallel: Regarding the typical MG (see Fig. 17) wherein

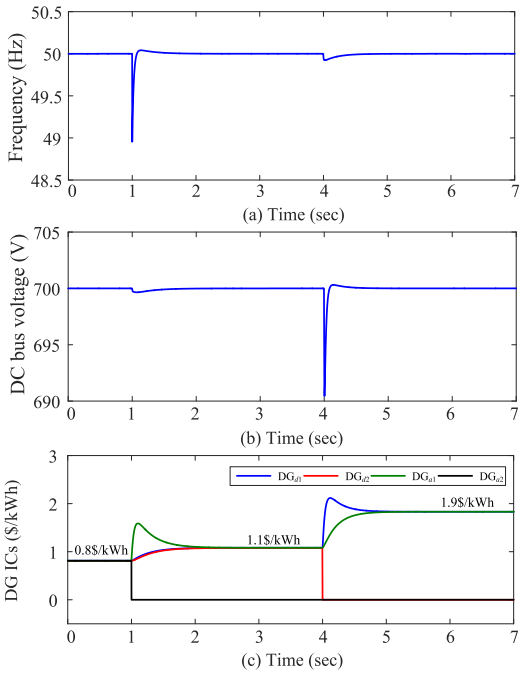

Fig. 12. The representative hybrid MG with DG_{a2} and DG_{d2} failures.

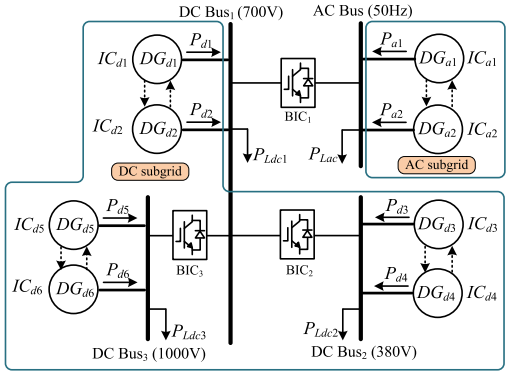

Fig. 13. A hybrid MG with multi-bus DC subgrid.

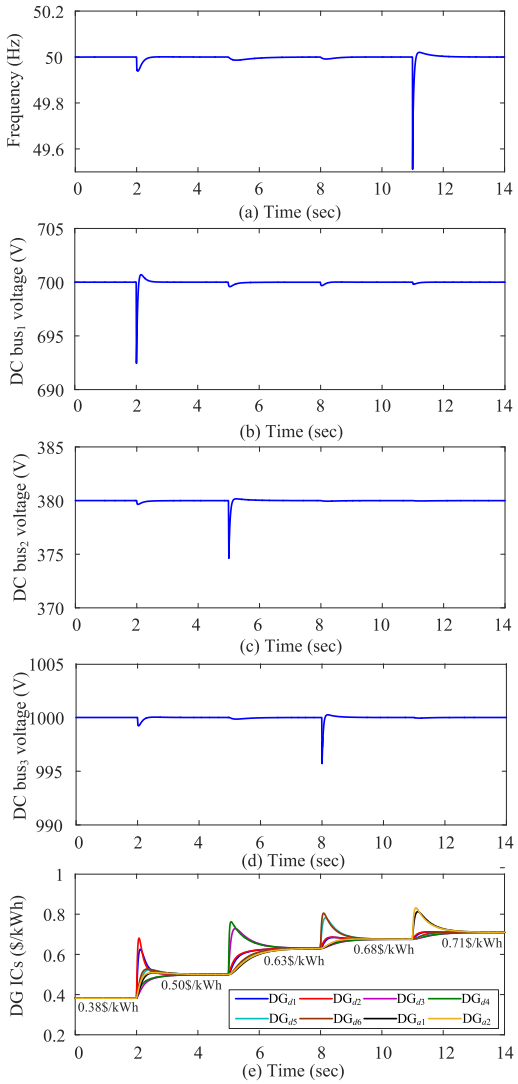

Fig. 14. Simulation results for Fig. 13.

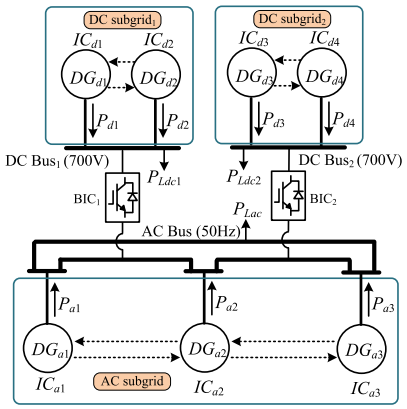

Fig. 15. A radially connected hybrid MG.

multiple DGs are integrated AC and DC buses in parallel, related simulations have been provided in Fig. 18. Resembling the former two systems, all DGs are with IC based droops, and the DCCFs in the subgrids drive AC frequency and DC voltage to their nominal values (50Hz, 700V). In the case of P_{Ldc} being augmented at 1s, the ICs of eight DGs shortly increase from 0.30$/kWh to 0.58$/kWh after system transition. At 6s, P_{Lac} step-up is enabled and all DG ICs quickly reach 0.73$/kWh. On these bases, it is conspicuous that, with the proposed strategy, the ICs equalization keeps independent of load changes.

V. Hardware in Loop (HIL) Verification

To experimentally validate the feasibility and effectiveness of the proposed distributed control architecture for global system economic operation in hybrid AC/DC MG. An in-house hardware in loop (HIL) testing platform is established, as in Fig. 19. The platform consists of a control board with DSP TMS23885, a RT-Lab OP5600 simulator, a host PC and an oscilloscope. The representative hybrid AC/DC MG shown in Fig. 9 and the first level controls for DGs are implemented in the RT-Lab simulator, whereas the proposed DCCF and the control algorithm of BIC are realized in DSP.

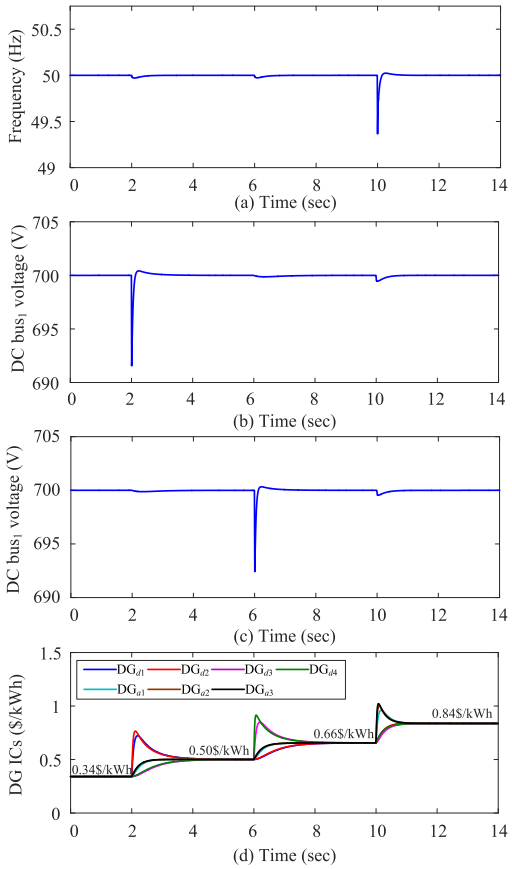

Fig. 16. Simulation results for Fig. 15.

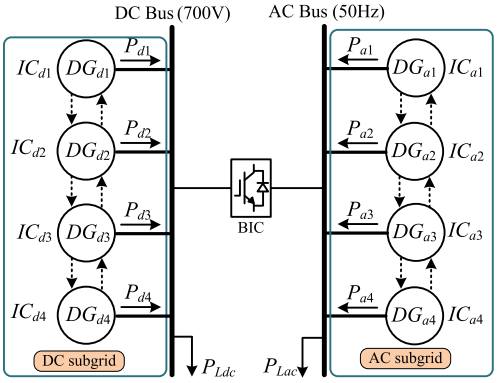

Fig. 17. A typical hybrid MG with multiple DGs in parallel connection.

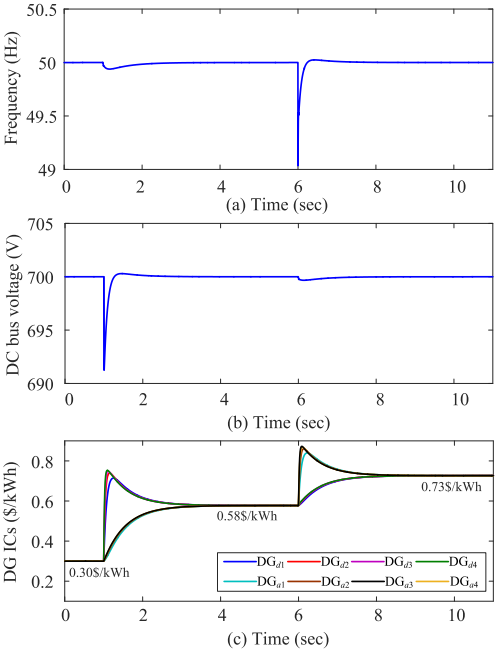

Fig. 18. Simulation results for Fig. 17.

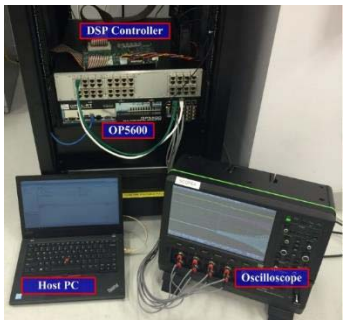

Fig. 19. HIL testing platform.

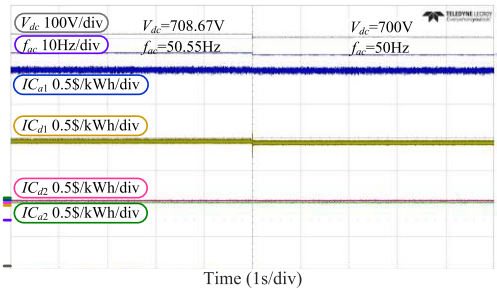

Fig. 20. HIL test stage 1: DCCF is enabled.

To conveniently explicate the validity of the proposed distributed architecture, HIL tests are divided into eight stages which are shown in TABLE III. From stage 1 to stage 7, the economic operation is achieved with the communication time delay of 20us, as reported in TABLE I. In stage 8, longer time delays are deliberately set to study the dynamic responses of the MG system.

As detailed in Fig. 20, at the beginning, DG_{a1} and DG_{d1} are in operation, while the other DGs and BIC are in idle mode. The initial AC frequency and DC bus voltage are 50.55Hz and 708.67V respectively. On the condition that the DCCF in the second level is activated, f_{ac} and V_{dc} are stably regulated at their nominal values, i.e., 50Hz and 700V. When BIC is enabled in stage 2, IC_{d1} and IC_{a1} immediately converge to 1.8$/kWh, which means the system operating cost is minimized even though the MG currently has only DG_{a1} and DG_{d1}, as plotted in Fig. 21.

According to Figs. 22-23, it is evident that the proposed distributed control architecture does allow PnP functionalities. In Fig. 22, DG_{d2} is unexpectedly integrated into the hybrid

TABLE III
HARDWARE IN LOOP TEST SEQUENCE

	DG_{d1}	DG_{d2}	DG_{a1}	DG_{a2}	BIC	DCCF	P_{Ldc} step up	P_{Lac} step up
Stage1	on	off	on	off	off	off → on	off	off
Stage2	on	off	on	off	off → on	on	off	off
Stage3	on	off → on	on	off	on	on	off	off
Stage4	on	on	on	off → on	on	on	off	off
Stage5	on	on	on	on	on	on	off → on	off
Stage6	on	on	on	on	on	on	on	off → on
Stage7	on	on	on	on	on	on → off	on	on
Stage8	on	on	on	on	on	off → on	off	off

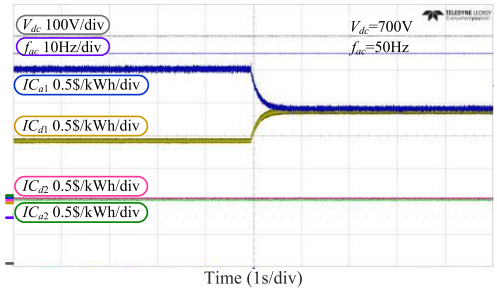

Fig. 21. HIL test stage 2: BIC is enabled.

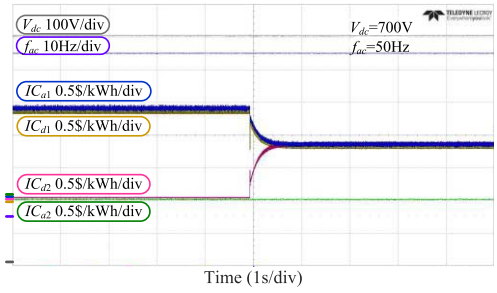

Fig. 22. HIL test stage 3: DG_{d2} is enabled.

MG. IC_{d1}, IC_{d2} and IC_{a1} quickly reach a level of ICs being around 0.8$/kWh. Once DG_{a2} is suddenly plugged into the MG, all DG ICs are equalized at about 0.6$/kWh after system transition. These results are consistent with the analyses in Section III-C, and global system economic operation of the studied hybrid AC/DC MG can thus be attained. Besides, it should be noted that f_{ac} and V_{dc} maintain at their respective nominal values no matter how MG system configuration varies.

Proceeding to Fig. 24 and Fig. 25, variations of all DG ICs could be found in the case that DC load P_{Ldc} and AC load P_{Lac} increase in sequence. When P_{Ldc} steps up firstly, DG ICs almost concurrently rise to the new optimal value which is estimated as 0.7$/kWh. When P_{Lac} step-up is also triggered, DG ICs remain at the same value in the steady state, and the newly-obtained IC is around 1$/kWh. In this sense, the overall system operating cost has been minimized.

Practically, the normal operation of MG system is threatened by considerable atrocious conditions. The attempt of this paper is to scrutinize the performances of the MG in the worst case that all communications fail and the entire second level

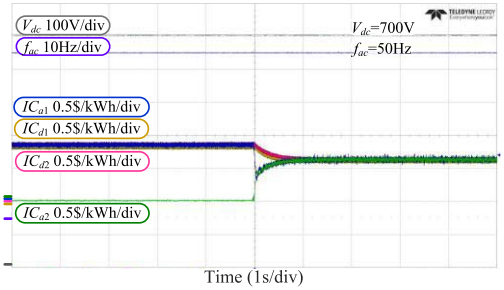

Fig. 23. HIL test stage 4: DG_{a2} is enabled.

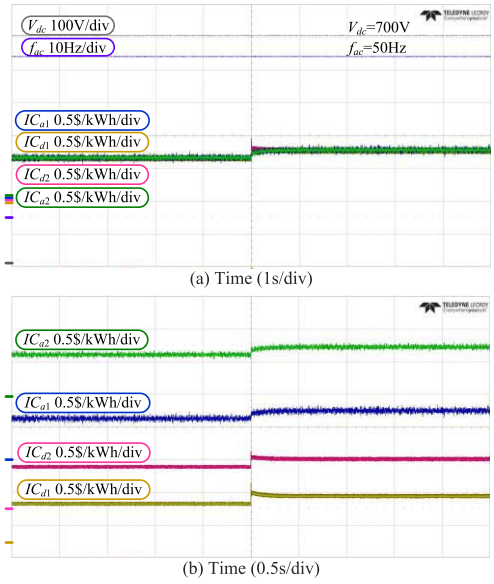

Fig. 24. (a) HIL test stage 5: P_{Ldc} steps up. (b) Zoomed view of ICs.

controls malfunction. In this context, f_{ac} and V_{dc} are unregulated and they would deviate from their nominal values. As plotted in Fig. 26, f_{ac} and V_{dc} shift to 50.79Hz and 708.7V after losing communication. Fortunately, all DG ICs still keep the same, which helps to maintain the global system economic operation.

Stage 1-7 have shown the steady operation of the MG system with communication time delay set as 20us. However, as mentioned early, the enlarged delay seriously poses a threat to the system stability. In stage 8, τ_d in is configured as 0.5s and 1s respectively, and the system dynamic responses are

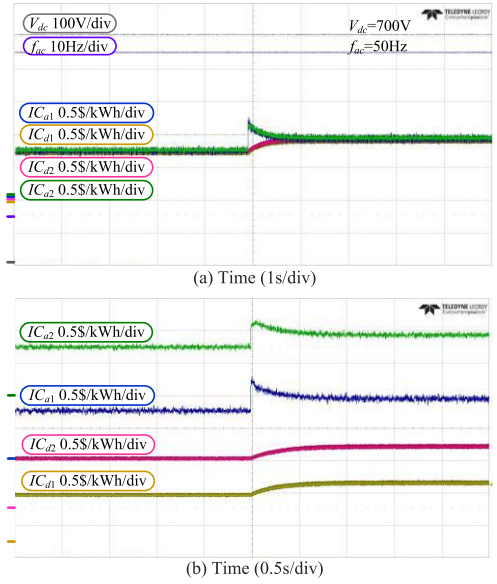

Fig. 25. (a) HIL test stage 6: P_{Lac} steps up. (b) Zoomed view of ICs.

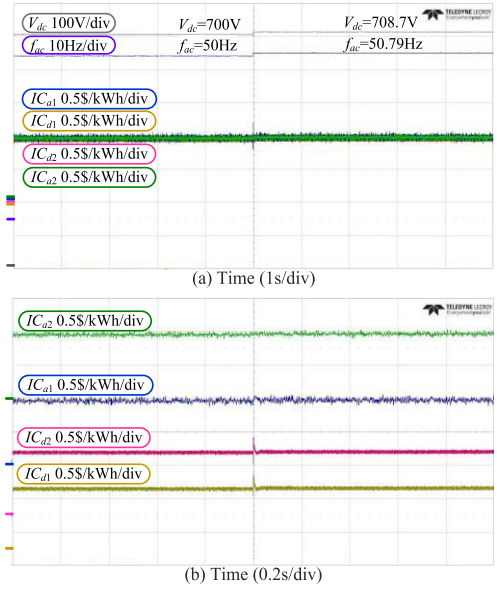

Fig. 26. (a) HIL test stage 7: DCCF is disabled and all communications fail. (b) Zoomed view of ICs.

accordingly displayed in Fig. 27 and Fig. 28. Initially, the loads step-up and the DCCF are all disabled, as expounded in TABLE III. In the case of $\tau_d = 0.5$s, when the second level control algorithms are exerted, large transient oscillations of DG ICs are observed, although the ICs maintain unaffected after 2s system transition. As seen from Fig. 27, the oscillation frequency is approximated as 5Hz, which is in good agreement with the stability analyses in Fig. 8. Next, in the situation that $\tau_d = 1$s, the whole system is unstable and oscillates at 3.5Hz. This result is also well supported by the related analyses in Section III-D, and for the hybrid AC/DC MG under study, the communication time delay should be less than 0.9s, as indicated by Fig. 8.

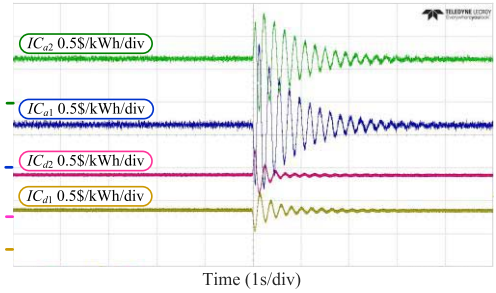

Fig. 27. HIL test stage 8: MG with communication delay of 0.5s.

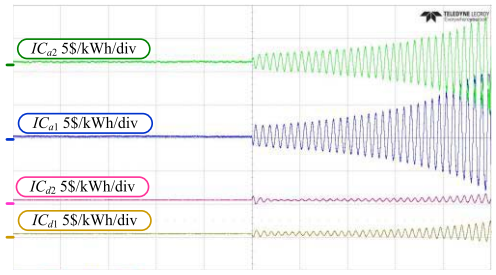

Fig. 28. HIL test stage 8: MG with communication delay of 1s.

VI. Conclusion

In this paper, a distributed control architecture is proposed for the global system economic operation of the hybrid AC/DC MG. The first level of the architecture implements IC based droop controllers in AC and DC subgrids. Although all DG ICs converge to the same value in the steady state, the adoption of droop schemes unavoidably causes f_{ac} and V_{dc} deviations. To benefit from the IC based droops and also achieve f_{ac} and V_{dc} recovery, in second control level, a DCCF, which can be uniformly applied to AC and DC subgrids, is proposed for regulating f_{ac} and V_{dc} to their nominal values. Due to the presence of DCCF, f_{ac} and V_{dc} maintain invariable. Hence, the loading conditions of AC and DC subgrids are invisible. To address this problem, an original RLI is proposed to extract the hidden loading status of each subgrid. With the RLI, the power reference of BIC can be easily defined. By properly scheduling the BIC, all DGs in the hybrid MG system will have the identical ICs in steady state, and the global system economic operation can thus be realized. Then, the impacts of communication time delay on overall stability are meticulously studied through a small signal model of a representative hybrid MG. Simulations and in-house HIL tests verify the feasibility and effectiveness of the proposed control architecture.

References

[1] F. Blaabjerg, R. Teodorescu, M. Liserre, and A. V. Timbus, "Overview of control and grid synchronization for distributed power generation systems," *IEEE Trans. Ind. Electron.*, vol. 53, no. 5, pp. 1398–1409, Oct. 2006.

[2] Z. Jiang and X. Yu, "Hybrid DC-and AC-linked microgrids: Towards integration of distributed energy resources," in *Proc. IEEE Energy 2030 Conf. ENERGY*, Atlanta, GA, USA, 2008, pp. 1–8.

[3] X. Liu, P. Wang, and P. C. Loh, "A hybrid AC/DC microgrid and its coordination control," *IEEE Trans. Smart Grid*, vol. 2, no. 2, pp. 278–286, Jun. 2011.

[4] K. S. Swarup and S. Yamashiro, "Unit commitment solution methodology using genetic algorithm," *IEEE Trans. Power Syst.*, vol. 17, no. 1, pp. 87–91, Feb. 2002.
[5] J.-Y. Fan and L. Zhang, "Real-time economic dispatch with line flow and emission constraints using quadratic programming," *IEEE Trans. Power Syst.*, vol. 13, no. 2, pp. 320–325, May 1998.
[6] C. Zhang, Y. Xu, Z. Y. Dong, and J. Ma, "Robust operation of microgrids via two-stage coordinated energy storage and direct load control," *IEEE Trans. Power Syst.*, vol. 32, no. 4, pp. 2858–2868, Jul. 2017.
[7] P. P. Vergara, J. C. López, M. J. Rider, and L. C. P. da Silva, "Optimal operation of unbalanced three-phase islanded droop-based microgrids," *IEEE Trans. Smart Grid*, to be published, doi: 10.1109/TSG.2017.2756021.
[8] M. M. A. Abdelaziz, H. E. Farag, E. F. El-Saadany, and Y. A.-R. I. Mohamed, "A novel and generalized three-phase power flow algorithm for islanded microgrids using a newton trust region method," *IEEE Trans. Power Syst.*, vol. 28, no. 1, pp. 190–201, Feb. 2013.
[9] F. Mumtaz, M. H. Syed, M. Al Hosani, and H. H. Zeineldin, "A novel approach to solve power flow for islanded microgrids using modified Newton Raphson with droop control of DG," *IEEE Trans. Sustain. Energy*, vol. 7, no. 2, pp. 493–503, Apr. 2016.
[10] H. Xin *et al.*, "A decentralized hierarchical control structure and self-optimizing control strategy for F-P type DGs in islanded microgrids," *IEEE Trans. Smart Grid*, vol. 7, no. 1, pp. 3–5, Jan. 2016.
[11] I. U. Nutkani, P. C. Loh, P. Wang, and F. Blaabjerg, "Cost-prioritized droop schemes for autonomous AC microgrids," *IEEE Trans. Power Electron.*, vol. 30, no. 2, pp. 1109–1119, Feb. 2015.
[12] I. U. Nutkani, P. C. Loh, P. Wang, and F. Blaabjerg, "Decentralized economic dispatch scheme with online power reserve for microgrids," *IEEE Trans. Smart Grid*, vol. 8, no. 1, pp. 139–148, Jan. 2017.
[13] I. U. Nutkani, P. C. Loh, P. Wang, and F. Blaabjerg, "Autonomous droop scheme with reduced generation cost," *IEEE Trans. Ind. Electron.*, vol. 61, no. 12, pp. 6803–6811, Dec. 2014.
[14] Q. Xu, J. Xiao, P. Wang, and C. Wen, "A decentralized control strategy for economic operation of autonomous AC, DC, and Hybrid AC/DC microgrids," *IEEE Trans. Energy Convers.*, vol. 32, no. 4, pp. 1345–1355, Dec. 2017.
[15] F. Chen *et al.*, "Cost-based droop schemes for economic dispatch in islanded microgrids," *IEEE Trans. Smart Grid*, vol. 8, no. 1, pp. 63–74, Jan. 2017.
[16] J. Xiao, P. Wang, and L. Setyawan, "Hierarchical control of hybrid energy storage system in DC microgrids," *IEEE Trans. Ind. Electron.*, vol. 62, no. 8, pp. 4915–4924, Aug. 2015.
[17] C. Jin, P. Wang, J. Xiao, Y. Tang, and F. H. Choo, "Implementation of hierarchical control in DC microgrids," *IEEE Trans. Ind. Electron.*, vol. 61, no. 8, pp. 4032–4042, Aug. 2014.
[18] J. M. Guerrero, M. Chandorkar, T.-L. Lee, and P. C. Loh, "Advanced control architectures for intelligent microgrids—Part I: Decentralized and hierarchical control," *IEEE Trans. Ind. Electron.*, vol. 60, no. 4, pp. 1254–1262, Apr. 2013.
[19] F. Guo, C. Wen, J. Mao, and Y.-D. Song, "Distributed secondary voltage and frequency restoration control of droop-controlled inverter-based microgrids," *IEEE Trans. Ind. Electron.*, vol. 62, no. 7, pp. 4355–4364, Jul. 2015.
[20] T. Dragièeviæ, J. M. Guerrero, and J. C. Vasquez, "A distributed control strategy for coordination of an autonomous LVDC microgrid based on power-line signaling," *IEEE Trans. Ind. Electron.*, vol. 61, no. 7, pp. 3313–3326, Jul. 2014.
[21] N. L. Diaz, J. C. Vasquez, and J. M. Guerrero, "A communication-less distributed control architecture for islanded microgrids with renewable generation and storage," *IEEE Trans. Power Electron.*, vol. 33, no. 3, pp. 1922–1939, Mar. 2018.
[22] A. J. Wood and B. F. Wollenberg, *Power Generation, Operation, and Control*, vol. 37. New York, NY, USA: Wiley, 1996.
[23] Y. A.-R. I. Mohamed and E. F. El-Saadany, "Adaptive decentralized droop controller to preserve power sharing stability of paralleled inverters in distributed generation microgrids," *IEEE Trans. Power Electron.*, vol. 23, no. 6, pp. 2806–2816, Nov. 2008.
[24] E. Rokrok and M. E. H. Golshan, "Adaptive voltage droop scheme for voltage source converters in an islanded multibus microgrid," *IET Gener. Transm. Distrib.*, vol. 4, no. 5, pp. 562–578, May 2010.
[25] P. C. Loh, D. Li, Y. K. Chai, and F. Blaabjerg, "Hybrid AC–DC microgrids with energy storages and progressive energy flow tuning," *IEEE Trans. Power Electron.*, vol. 28, no. 4, pp. 1533–1543, Apr. 2013.
[26] C. Godsil and G. F. Royle, *Algebraic Graph Theory* (Graduate Texts in Mathematics), vol. 207. New York, NY, USA: Springer-Verlag, 2001.
[27] P. Wang *et al.*, "Distributed control for autonomous operation of a three-port AC/DC/DS hybrid microgrid," *IEEE Trans. Ind. Electron.*, vol. 62, no. 2, pp. 1279–1290, Feb. 2015.
[28] P. C. Loh, D. Li, Y. K. Chai, and F. Blaabjerg, "Autonomous operation of hybrid microgrid with AC and DC subgrids," *IEEE Trans. Power Electron.*, vol. 28, no. 5, pp. 2214–2223, May 2013.
[29] J. Lai, H. Zhou, X. Lu, X. Yu, and W. Hu, "Droop-based distributed cooperative control for microgrids with time-varying delays," *IEEE Trans. Smart Grid*, vol. 7, no. 4, pp. 1775–1789, Jul. 2016.
[30] T. Dragièević, J. M. Guerrero, J. C. Vasquez, and D. Škrlec, "Supervisory control of an adaptive-droop regulated DC microgrid with battery management capability," *IEEE Trans. Power Electron.*, vol. 29, no. 2, pp. 695–706, Feb. 2014.
[31] J. He and Y. W. Li, "Analysis, design, and implementation of virtual impedance for power electronics interfaced distributed generation," *IEEE Trans. Ind. Appl.*, vol. 47, no. 6, pp. 2525–2538, Nov./Dec. 2011.
[32] S. Yang, S. Tan, and J.-X. Xu, "Consensus based approach for economic dispatch problem in a smart grid," *IEEE Trans. Power Syst.*, vol. 28, no. 4, pp. 4416–4426, Nov. 2013.
[33] Y. Xu and Z. Li, "Distributed optimal resource management based on the consensus algorithm in a microgrid," *IEEE Trans. Ind. Electron.*, vol. 62, no. 4, pp. 2584–2592, Apr. 2015.
[34] F. Guo, C. Wen, J. Mao, and Y.-D. Song, "Distributed economic dispatch for smart grids with random wind power," *IEEE Trans. Smart Grid*, vol. 7, no. 3, pp. 1572–1583, May 2016.
[35] Z. Zhang and M.-Y. Chow, "Convergence analysis of the incremental cost consensus algorithm under different communication network topologies in a smart grid," *IEEE Trans. Power Syst.*, vol. 27, no. 4, pp. 1761–1768, Nov. 2012.
[36] Z. Yang, J. Xiang, and Y. Li, "Distributed consensus based supply–demand balance algorithm for economic dispatch problem in a smart grid with switching graph," *IEEE Trans. Ind. Electron.*, vol. 64, no. 2, pp. 1600–1610, Feb. 2017.

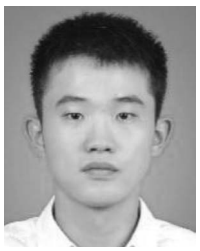

Pengfeng Lin (S'16) received the B.S. and M.S. degrees in electrical engineering from Southwest Jiaotong University, China, in 2013 and 2015, respectively. He is currently pursuing the Ph.D. degree with Interdisciplinary Graduate School, ERI@N, Nanyang Technological University, Singapore. His research interests include energy storage systems and hybrid ac/dc microgrids.

Chi Jin received the B.Sc. degree in electrical engineering from Wuhan University, Wuhan, China, in 2007 and the M.Sc. and Ph.D. degrees from the School of Electrical and Electronic Engineering, Nanyang Technological University, Singapore, in 2008 and 2013, respectively.

In 2011, he was a Visiting Scholar with the Institute of Energy Technology, Aalborg University, Aalborg East, Denmark, where he worked on the control strategies of hybrid ac/dc/storage microgrid system. Since 2013, he has been with the Energy Research Institute, Nanyang Technological University as a Research Fellow.

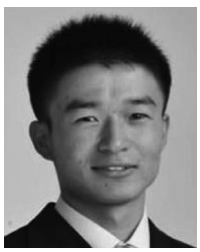

Jianfang Xiao (S'11–M'16) received the B.Sc. degree (First-Class Hons.) in mechanical engineering from the School of Mechanical and Aerospace Engineering, Nanyang Technological University (NTU), in 2011 and the Ph.D. degree in electrical engineering from the School of Electrical and Electronic Engineering, NTU, in 2015, where he is currently a Research Fellow with the Energy Research Institute.

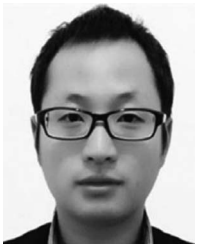

Xiaoqiang Li (M'16) received the B.S. degree in electrical engineering and automation and the Ph.D. degree in electrical engineering from the School of Information and Electrical Engineering, China University of Mining and Technology, Xuzhou, China, in 2010 and 2015, respectively. From 2015 to 2018, he was a Research Fellow with Nanyang Technological University, Singapore. Since 2018, he has been with the China University of Mining and Technology, Xuzhou, as an Associate Professor. His current research interests include renewable energy generation and digital control in power electronics.

Donghan Shi received the B.Eng. degree in electrical engineering from Wuhan University, Wuhan, China, in 2013 and the M.Sc. degree from the School of Electrical and Electronic Engineering, Nanyang Technological University (NTU), Singapore, in 2014. Since 2014, he has been with NTU as a Research Associate and currently he is with Energy Research Institute.

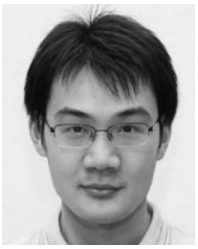

Yi Tang (S'10–M'14) received the B.Eng. degree in electrical engineering from Wuhan University, Wuhan, China, in 2007 and the M.Sc. and Ph.D. degrees from the School of Electrical and Electronic Engineering, Nanyang Technological University (NTU), Singapore, in 2008 and 2011, respectively.

From 2011 to 2013, he was a Senior Application Engineer with Infineon Technologies Asia Pacific, Singapore. From 2013 to 2015, he was a Post-Doctoral Research Fellow with Aalborg University, Aalborg, Denmark. Since 2015, he has been with NTU, as an Assistant Professor. He is the Cluster Director in advanced power electronics research program with Energy Research Institute, NTU.

Dr. Tang was a recipient of the Infineon Top Inventor Award in 2012 and the Early Career Teaching Excellence Award in 2017. He serves as an Associate Editor for the IEEE JOURNAL OF EMERGING AND SELECTED TOPICS IN POWER ELECTRONICS.

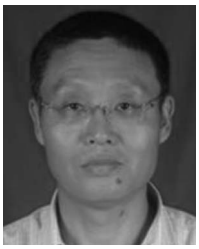

Peng Wang (M'00–SM'11–F'18) received the B.Sc. degree from Xian Jiaotong University, China, in 1978, the M.Sc. degree from the Taiyuan University of Technology, China, in 1987, and the M.Sc. and Ph.D. degrees from the University of Saskatchewan, Canada, in 1995 and 1998, respectively. He is currently a Professor with Nanyang Technological University, Singapore.